

Towards self-organization of decaying surface corrugations: A numerical study

Andrea Bonito,^{1,2} Ricardo H. Nochetto,^{2,3} John Quah,² and Dionisios Margetis^{2,3}

¹*Department of Mathematics, Texas A&M University, College Station, Texas 77843, USA*

²*Department of Mathematics, University of Maryland, College Park, Maryland 20742, USA*

³*Institute for Physical Science and Technology, University of Maryland, College Park, Maryland 20742, USA*

(Dated: April 24, 2009)

We study numerically the interplay of *surface topography* and *kinetics* in the relaxation of crystal surface corrugations below roughening in two independent space dimensions. The kinetic processes are *isotropic* diffusion of adatoms across terraces and attachment-detachment of atoms at steps. We simulate the corresponding *anisotropic* partial differential equation for the surface height via the *finite element method*. The numerical results show a sharp transition from initially bi-periodic surface profiles to one-dimensional surface morphologies. This transition is found to be enhanced by an applied electric field. Our predictions demonstrate the dramatic influence on morphological relaxation of *geometry-induced* asymmetries in the adatom fluxes transverse and parallel to step edges.

PACS number(s): 68.35.Ja, 68.35.Md, 81.15.Aa, 02.70.Dh

The drive towards fabrication of nanostructures for data and energy storage, computing and sensor arrays has stimulated active interest in the self-assembly and self-organization of crystal surface structures. A common practice for realizing these phenomena is to use templates on which each nanostructure evolves controllably. The template production requires understanding how various competing factors such as geometric, kinetic and energetic effects can be *tuned* to direct self-organization [1].

Below the roughening temperature, the cause of crystal surface morphological evolution is the microscale motion of steps [2, 3]. These move by mass conservation as adsorbed atoms (adatoms) diffuse on nanoscale terraces, and attach-detach at step edges. The combined effect of *topography* and *kinetics* underlies observations of decaying surface corrugations [4–6].

Our starting point is a partial differential equation (PDE) for the surface height profile. This PDE was *derived* from the motion of steps in two independent space dimensions (2D) [7, 8]. Its distinct ingredient, which is absent from previous continuum treatments (e.g. [9–11]), is the *tensorial* mobility relating the large-scale adatom flux to the step chemical potential gradient. This anisotropy *emerges* as a *geometric* effect from coarse-graining different microscale fluxes transverse and parallel to steps, even if the physics of terraces is isotropic.

In this Rapid Communication, we study numerically this new relaxation PDE via the finite element method (FEM) in a 2D periodic setting. We emphasize *universal* (non-sensitive to material details) aspects of surface relaxation. A prominent prediction from our simulations is a *topographic transition*: a sharp passage from 2D to almost one-dimensional (1D) surface profiles at finite times. This transition is controlled by: (i) the surface aspect ratio; (ii) the material kinetic parameters; and (iii) an applied electric field. Most other continuum relaxation treatments rely on a *scalar* surface mobility. Our PDE theory (stemming directly from coarse-graining

steps in 2D) embodies the distinct behaviors of fluxes normal and parallel to step edges and, thus, allows for a geometry-induced bias of evolution to 1D morphologies.

Model. The PDE for the height, $h(x, y, t)$, is [7, 8]

$$\partial_t h = B \nabla \cdot \left\{ \mathbf{\Lambda} \cdot \nabla \left[\frac{g_1}{g_3} \nabla \cdot \left(\frac{\nabla h}{|\nabla h|} \right) + \nabla \cdot (|\nabla h| \nabla h) \right] \right\}, \quad (1)$$

where $\nabla = (\partial_x, \partial_y)$, $B = \frac{D_s C_s g_3 \Omega^2}{k_B T}$ (length⁴/time), D_s is the (scalar) terrace diffusivity, C_s is the equilibrium adatom density at a straight step, and $\mathbf{M} = -\frac{D_s}{k_B T} \mathbf{\Lambda}$ is the tensor mobility (length²/energy/time); g_1 expresses the step line tension, g_3 expresses entropic and elastic dipole step interactions, and Ω is the atomic volume. Note that (by $h_x := \partial_x h$)

$$\mathbf{\Lambda} = -\mathbf{S} \begin{pmatrix} \frac{1}{1+q|\nabla h|} & 0 \\ 0 & 1 \end{pmatrix} \mathbf{S}^T, \quad \mathbf{S} = \begin{pmatrix} \frac{h_x}{|\nabla h|} & -\frac{h_y}{|\nabla h|} \\ \frac{h_y}{|\nabla h|} & \frac{h_x}{|\nabla h|} \end{pmatrix}, \quad (2)$$

where $q = \frac{2D_s}{ka}$ and k is the kinetic rate of atom attachment-detachment at steps [3]. Equation (1) is the limit of step dynamics outside facets, i.e., macroscopically flat surface regions. Furthermore, Eq. (1) holds in a variational sense for all ∇h and ensures the fastest decrease of the surface free energy $E = \int dA [g_1 |\nabla h| + (g_3/3) |\nabla h|^3]$ ($dA = dx dy$), which comes from a small-slope expansion for the step energy density [3]. PDE (1) can also be derived via: (i) the chemical potential $\mu = \Omega(\delta E/\delta h)$, the *variation* of E ; (ii) the constitutive law $\mathbf{J} = -C_s \mathbf{M} \cdot \nabla \mu$; and (iii) mass conservation, $\partial_t h + \Omega \mathbf{J} = 0$, where \mathbf{J} is the adatom flux. Equation (2) for $\mathbf{\Lambda}$ (and \mathbf{M}) comes directly from coarse-graining the step kinetics [7, 8].

Numerical method. We exploit this variational framework to simulate PDE (1) by using the FEM in space [12] and finite differences in time. PDE (1) is split into two equations: one for the height h , from mass conservation and the constitutive law for \mathbf{J} , and another for the chemical potential μ , the variational derivative of the energy

functional $E[h]$. We apply a semi-implicit Euler scheme to express Eq. (1) as a system in the updated variables (h^{n+1}, μ^{n+1}) where $h^n \approx h(\cdot, n\tau^n)$ and τ^n is the (adaptive) time step. The mobility \mathbf{M} and the energy $E[h]$ are evaluated by use of (h^n, μ^n) to ensure *linearity* with (h^{n+1}, μ^{n+1}) . We apply periodic boundary conditions in the box $\mathcal{B} = [0, \lambda_1] \times [0, \lambda_2]$: the initial data for h is periodic with wavelengths λ_1, λ_2 (in x and y). The equations for h and μ are recast to their “weak form”, i.e., via multiplication by a periodic test function ϕ and integration by parts over \mathcal{B} . If $g_1 = 0$ the FEM equations for (h, μ) read

$$\int dA [\mu^{n+1} \phi - \Omega g_3 |\nabla h^n| \nabla h^{n+1} \cdot \nabla \phi] = 0, \quad (3)$$

$$\int dA \left[\frac{h^{n+1} - h^n}{\tau} \phi + M^\epsilon (\nabla h^n) \nabla \mu^{n+1} \cdot \nabla \phi \right] = 0, \quad (4)$$

where h^{n+1} and μ^{n+1} are continuous piecewise linear, and $M^\epsilon(\nabla h)$ is a regularized mobility.

An issue is that μ (for $g_1 \neq 0$) and \mathbf{S} (and thus \mathbf{M}) computed directly from derivatives of h are ill-defined as $\nabla h \rightarrow 0$. To circumvent this difficulty, we regularize the ∇h -dependent terms in question by *analytic* expressions having a small positive parameter, ϵ . We apply three different regularization schemes, all of which give practically identical results [16]. (A scheme for μ similar to one of our schemes is used in [13–15] with a scalar mobility.)

Other numerical treatments of surface relaxation in 2D invoke the scalar mobility $M_0 = \frac{D_s}{k_B T} (1 + q|\nabla h|)^{-1}$ [9–11, 15]. Noteworthy are Fourier series expansions for the height profile [10, 11, 17], which yield nonlinear differential equations for the requisite coefficients. Our FEM approach is of similar variational nature, is of low order in space, and offers the computational advantage of solving the linear system of Eqs. (3), (4).

The FEM variational description is consistent with the near-equilibrium step dynamics in the absence of facets (if $g_1 = 0$) [18]. The collapse of individual steps on top of facets influence the surface profile macroscopically via a microscale condition at the facet free boundary [18, 19], which is not included in the FEM or previous variational methods [9–11]. This case is further discussed below.

We now discuss our numerical method for $g_1 = 0$, i.e., without facets. As a criterion for terminating each simulation we require that $R_1 < \delta_1$, where $R_1 = h_m(t)/h_0$ is the ratio of the maximum height, $h_m(t)$, to the initial height peak, h_0 , and δ_1 is given ($\delta_1 \ll 1$). For comparison purposes, we simulate Eq. (1) both for $\mathbf{M} = M_0 \mathbf{1}$ (“scalar case”) [9–11] and the tensor \mathbf{M} of Eq. (2) (“tensor case”); see Fig. 1. The time dependence of the height peak $h_m(t)$ and surface energy $E(t)$ are shown in Fig. 2.

For the tensor case, a prominent feature of surface relaxation from our numerics is the *sharp transition* of a fully 2D morphology to an almost 1D surface height profile (see Fig. 1). The final profile is along the (y -

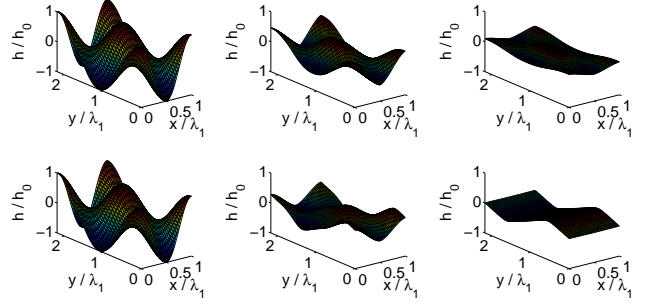


FIG. 1: (Color online) Relaxing height profile in box \mathcal{B} (t increases from left to right); $g_1 = 0$, $q = 10^4$, $h(x, y, 0) = h_0 \cos(k_1 x) \cos(k_2 y)$, $k_2/k_1 = \lambda_1/\lambda_2 = 11/24$. Top: Scalar case, where the 2D structure of the initial profile is preserved. Bottom: Tensor case, where a transition to an almost 1D profile occurs.

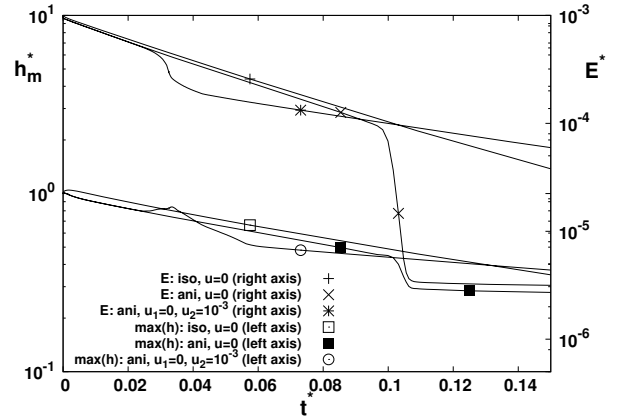


FIG. 2: Log plots for nondimensional maximum height, $h_m^*(t) = h_m(t)/h_0$ (left axis), and nondimensional surface energy, $E^*(t) = E(t)\lambda_x^2/(h_0^3 g_3 \lambda_y)$ (right axis), vs nondimensional time $t^* = tk_B T \lambda_1^5/(h_0 D_s C_s g_3 \Omega^2)$, for scalar (iso) and tensor (ani) cases without and with electric field (drift velocity $\mathbf{v} \neq 0$ in Eq. (5)); $g_1 = 0$, $q = 10^4$, $h(x, y, 0) = h_0 \cos(k_1 x) \cos(k_2 y)$, $k_2/k_1 = \lambda_1/\lambda_2 = 11/24$, $\mathbf{u} = (0, u_2) = \lambda_1 \mathbf{v}/D_s$ and $\delta_1 = 10^{-5}$. The presence of electric field causes an earlier transition (see Figs. 3 and 4).

direction of the *largest* wavelength (λ_2). The corresponding decay for the maximum height and surface energy *switches abruptly* from an exponential behavior to another, as shown in Fig. 2. This change occurs at the time of the topographic transition. By contrast, the scalar mobility preserves the 2D structure of the initial profile.

To detect reliably a transition in simulations, we quantify how close the height profile is to a perfectly 1D morphology. So, we define the geometric ratio $R_2 = \int_{\mathcal{B}} dA (h_x)^2 / \int_{\mathcal{B}} dA (h_y)^2$. We assert that a transition occurs in the numerics if we find $R_2 < \delta_2$ while $R_1 \geq \delta_1$ (where δ_1 and δ_2 are chosen sufficiently small).

Effect of parameters. We now explore how the transition is affected by the aspect ratio $\alpha = \lambda_1/\lambda_2$ and the material parameter q . For definiteness, consider $0 < \alpha < 1$.

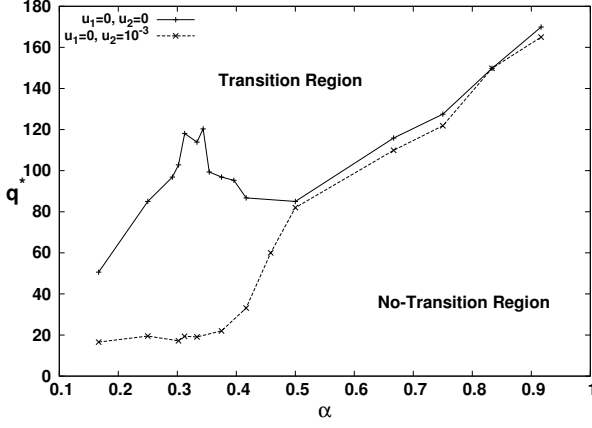


FIG. 3: Threshold values of (scaled) parameter $q^* = qh_0/\lambda_1$ vs domain aspect ratio $\alpha = \lambda_1/\lambda_2 = k_2/k_1$ for a transition to occur, in the absence (solid line) and presence (dashed line) of electric field \mathbf{E}_e in the y -direction (drift velocity $\mathbf{v} \neq 0$ and $\mathbf{u} = (0, u_2) = \lambda_1 \mathbf{v}/D_s$). The downward shift of the threshold q^* -curve indicates the enhancement by \mathbf{E}_e of the transition. Transition is prohibited (permitted) for values of q^* 3 units below (above) each curve, with $\delta_1 = \delta_2 = 10^{-3}$.

With fixed α , δ_1 and δ_2 , the transition is *suppressed* by the decrease of q , since the mobility \mathbf{M} approaches a constant diagonal tensor. So, we expect that for given α a transition occurs only if q exceeds a threshold, $q_{th}(\alpha)$. This claim is verified by our numerics. Interestingly, the computed $h_0 q_{th}(\alpha)/\lambda_1$ is *non-monotonic*, having a local maximum at $\alpha \approx 0.3$, as shown in Fig. 3. An explanation of this behavior is as yet elusive.

Our observations motivate the question: *What is the precise cause of the transition?* An analytic answer is not clear to us at the moment. We recognize that the tensor character of the mobility has an appreciable effect on the relative magnitudes of the adatom fluxes normal and parallel to step edges. In the scalar case, the predominant flux component is always normal to step edges, inducing *isotropic* changes to the height level sets (curves where $h = \text{const.}$). By contrast, in the tensor case the longitudinal flux prevails initially, apparently following the geometry of the level sets (see Fig. 4). The transition seems to be correlated with the onset of a significant normal flux, which accompanies the gradual *mergence* of adjacent height level sets. This behavior is accentuated by the decrease of the aspect ratio, α (see Fig. 3).

Effect of electric field. The role of asymmetry in the adatom fluxes for the tensor case can be demonstrated via application of a constant electric field, \mathbf{E}_e . The idea is to reinforce fluxes of charged adatoms in a prescribed direction and, thus, accelerate the observed transition. Further, the electric field is a common controllable parameter in experimental settings (see, e.g., [20]).

The \mathbf{E}_e -field is incorporated directly in PDE (1) leaving essentially intact its variational structure. Main ingredients of the new PDE remain the chemical potential

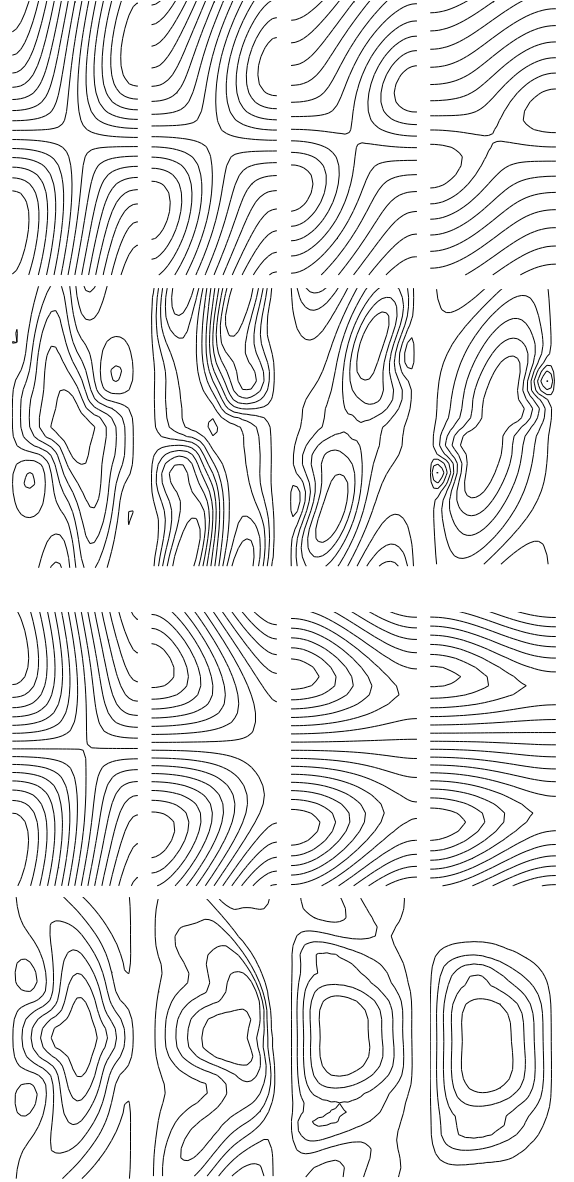


FIG. 4: Snapshots of height level sets (first and third rows) and adatom vector flux streamlines, i.e., curves tangential to flux (second and fourth rows) during transition, shown in the box $[0, \lambda_1/2] \times [0, \lambda_2/2]$. Streamlines are *not* normal to level sets, thereby reflecting the tensor nature of mobility, and exhibit a tendency to align with the y -axis for increasing time (from left to right). Upper two rows: $\mathbf{E}_e = 0$. Lower two rows: $\mathbf{E}_e \neq 0$ in y -direction with $|\mathbf{u}| = \lambda_1 |\mathbf{v}|/D_s = 10^{-3}$ (see Eq. (5)). Parameter values: $g_1 = 0$, $q = 10^4$, $h(x, y, 0) = h_0 \cos(k_1 x) \cos(k_2 y)$, $k_2/k_1 = 11/24$. The time scale for $\mathbf{E}_e \neq 0$ is shorter than for $\mathbf{E}_e = 0$ (see also Fig. 2).

$\mu = \Omega(\delta E/\delta h)$ (E : surface free energy) and the mass conservation law $\partial_t h + \Omega \nabla \cdot \mathbf{J} = 0$. However, the relation between \mathbf{J} , the surface flux, and μ now becomes [21]

$$\mathbf{J} = -C_s \mathbf{M} \cdot \left[\nabla \mu - \frac{k_B T}{D_s} \mathbf{v} \left(1 + \frac{\mu}{k_B T} \right) \right], \quad (5)$$

where $\mathbf{v} = D_s |Z^* e| \mathbf{E}_e / (k_B T)$ is the drift velocity and

Z^*e is the effective adatom charge [20]. Hence, the PDE acquires a convective (linear in \mathbf{v}) term. If $\mathbf{u} = \lambda_1 \mathbf{v}/D_s$ is the nondimensional velocity and ρ is the meshsize, then the numerical Péclet number $P_e = \rho|\mathbf{v}|/D_s = \rho|\mathbf{u}|/\lambda_1$ quantifies the relative importance of convection to diffusion. In most applications with semiconductor surfaces, $P_e \ll 1$ [20]. Details on our numerics can be found in [16].

We take \mathbf{E}_e in the y -direction, of the largest wavelength, to reinforce the fluxes in this direction (see Fig. 2). The threshold $q_{th}(\alpha; \mathbf{E}_e)$ decreases with $|\mathbf{E}_e|$ and *exhibits a plateau for small α* (in striking contrast with the case $\mathbf{E}_e = 0$), as shown in Fig. 3. This indicates that varying the aspect ratio α (for a fixed material) can lead to a fast and sharp topographic transition via suitable tuning of \mathbf{E}_e . This prediction may be *testable experimentally*.

Open questions. Our numerics are restricted to situations with step line tension $g_1 = 0$, *without facets*. Preliminary computations by the FEM indicate that the transition persists *continuously* with nonzero yet small g_1 , as shown in Fig. 5. Theoretical understanding of the transition for any g_1 is still lacking. A study of $g_1 \neq 0$ strictly requires the incorporation into the variational framework of a microscale condition for the collapse times of individual steps [18, 19]. This task calls for a hybrid (discrete/continuum) approach.

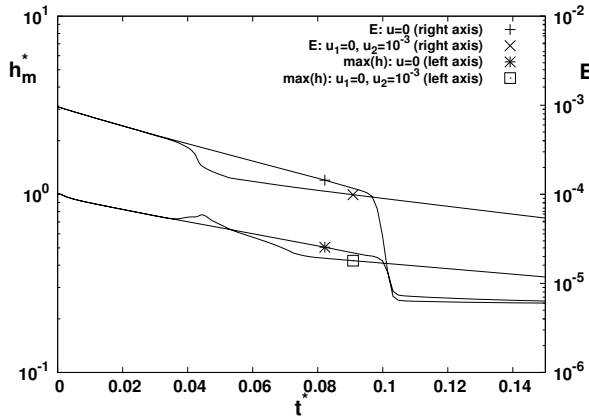


FIG. 5: Log plots for nondimensional maximum height, $h_m^*(t) = h_m(t)/h_0$ (left axis), and nondimensional surface energy, $E^*(t) = E(t)\lambda_x^2/(h_0^3 g_3 \lambda_y)$ (right axis), for tensor case *with facets*: $(g_1/g_3)(\lambda_1/h_0)^2 = 10^{-4}$, $q = 10^4$, and $h(x, y, 0) = h_0 \cos(k_1 x) \cos(k_2 y)$, $k_2/k_1 = \lambda_1/\lambda_2 = 11/24$, and $\delta_1 = 10^{-5}$, $\delta_2 = 0$.

It is of interest to test our simulations against experiments of decaying surface corrugations. Available data for relaxing Si surface profiles with different aspect ratios and $\mathbf{E}_e = 0$ [4–6] suggest that the parameter α plays a key role in the height decay. Similar experiments may be carried out for *nonzero* \mathbf{E}_e , possibly enabling a transition. A perhaps more appealing candidate system is GaAs. Step parameters such as g_1 and g_3 are not widely known for GaAs surfaces [22]. Experimental observations [23] indicate that GaAs(001) undergoes

a pre-roughening transition at a temperature close to 500°C, at which g_1/g_3 becomes small. It is conceivable to use our predictions to relate observed decay rates and possible transition times with material parameters, e.g. g_1/g_3 , and thereby estimate these parameters for GaAs.

We thank R. D. James, R. V. Kohn, and R. J. Phaneuf for valuable discussions. A.B.’s research was supported by NSF via Grant No. DMS-0505454. R.H.N.’s research was supported by NSF via Grants No. DMS-0505454 and DMS-0807811. J.Q. had the financial support of Monroe Martin at the University of Maryland. D.M.’s research was supported by NSF-MRSEC via Grant No. DMR-0520471 at the University of Maryland.

-
- [1] T. Michely and J. Krug, *Islands, Mounds and Atoms: Patterns and Processes in Crystal Growth Far From Equilibrium* (Springer-Verlag, Berlin, 2004).
 - [2] W. K. Burton, N. Cabrera, and F. C. Frank, *Philos. Trans. R. Soc. London Ser. A* **243**, 299 (1951).
 - [3] H.-C. Jeong and E. D. Williams, *Surf. Sci. Rep.* **34**, 171 (1999).
 - [4] M. E. Keefe, C. C. Umbach, and J. M. Blakely, *J. Phys. Chem. Solids* **55**, 965 (1994).
 - [5] J. Erlebacher, M. J. Aziz, E. Chason, M. B. Sinclair, and J. A. Floro, *Phys. Rev. Lett.* **84**, 5800 (2000).
 - [6] L. Pedemonte, G. Bracco, C. Boragno, F. Buatier de Mongeot, and U. Valbusa, *Phys. Rev. B* **68**, 115431 (2003).
 - [7] D. Margetis, *Phys. Rev. B* **76**, 193403 (2007).
 - [8] D. Margetis and R. V. Kohn, *Multiscale Model. Simul.* **5**, 729 (2006).
 - [9] D. Margetis, M. J. Aziz, and H. A. Stone, *Phys. Rev. B* **69**, 041404 (2004); *Phys. Rev. B* **71**, 165432 (2005).
 - [10] V. B. Shenoy, A. Ramasubramaniam, H. Ramanarayan, D. T. Tambe, W. L. Chan, and E. Chason, *Phys. Rev. Lett.* **92**, 256101 (2004).
 - [11] W. L. Chan, A. Ramasubramaniam, V. B. Shenoy, and E. Chason, *Phys. Rev. B* **70**, 245403 (2004).
 - [12] D. Braess, *Finite Elements: Theory, Fast Solvers, and Applications in Solid Mechanics* (Cambridge University Press, New York, 2nd Ed., 2001).
 - [13] H. P. Bonzel, E. Preuss, and B. Steffen, *Appl. Phys. A: Solids Surf.* **35**, 1 (1984); *Surf. Sci.* **145**, 20 (1984).
 - [14] H. P. Bonzel and E. Preuss, *Surf. Sci.* **336**, 209 (1995).
 - [15] M. V. R. Murty, *Phys. Rev. B* **62**, 17004 (2000).
 - [16] A. Bonito, D. Margetis, and R. H. Nochetto, to be published.
 - [17] V. B. Shenoy and L. B. Freund, *J. Mech. Phys. Solids* **50**, 1817 (2002).
 - [18] D. Margetis, P.-W. Fok, M. J. Aziz, and H. A. Stone, *Phys. Rev. Lett.* **97**, 096102 (2006).
 - [19] N. Israeli and D. Kandel, *Phys. Rev. B* **60**, 5946 (1999).
 - [20] E. S. Fu, D.-J. Liu, M. D. Johnson, J. D. Weeks, and E. D. Williams, *Surf. Sci.* **385**, 259 (1997).
 - [21] J. Quah and D. Margetis, to be published.
 - [22] M. Itoh, *Prog. Surf. Sci.* **66**, 53 (2001).
 - [23] Z. Ding, D. W. Bullock, P. M. Thibado, V. P. LaBella, and K. Mullen, *Phys. Rev. Lett.* **90**, 216109 (2003).